Light-Induced Exciton Spin Hall Effect in van der Waals Heterostructures

Yun-Mei Li,[1] Jian Li,[1] Li-Kun Shi,[2] Dong Zhang,[1] Wen Yang,[2] and Kai Chang[1,3,*]
[1]SKLSM, Institute of Semiconductors, Chinese Academy of Sciences, P.O. Box 912, Beijing 100083, China
[2]Beijing Computational Science Research Center, Beijing 100094, China
[3]Synergetic Innovation Center of Quantum Information and Quantum Physics, University of Science and Technology of China, Hefei, Anhui 230026, China

(Received 12 June 2015; revised manuscript received 21 August 2015; published 15 October 2015)

We propose a light-induced spin Hall effect for interlayer exciton gas in monolayer $MoSe_2$-WSe_2 van der Waals heterostructure. By applying two infrared, spatially varying laser beams coupled to the exciton internal states, a spin-dependent gauge potential on the exciton center-of-mass motion is induced. This gauge potential deflects excitons in different spin states towards opposite directions, leading to a finite spin current but vanishing mass current. In the Hall bar geometry, the spin-dependent deflection gives rise to spin-dependent chiral edge states with spin-velocity locking. The spin current and chiral edge states of the excitons can be detected by spatially resolved photoluminescence spectroscopy.

DOI: 10.1103/PhysRevLett.115.166804 PACS numbers: 73.43.-f, 71.35.Cc, 72.25.-b

Two-dimensional (2D) layered transition metal dichalcogenides (TMDs), such as MoS_2 and WSe_2, are emerging as promising candidates for next-generation optoelectronics [1–4] and as a new platform for exploring novel physics in 2D systems [5–9]. In contrast to graphene, TMD 2D materials possess direct band gaps tuned by composition, structure, and dimensionality. The optical properties of monolayer TMD are characterized by two polarization-selective, low-energy exciton peaks that arise from vertical transitions from the spin-orbit-split valence band to the doubly degenerate conduction band in the $\pm\mathbf{K}$ valleys of the Brillouin zone [1,2,10,11]. The reduced dielectric screening in gapped 2D systems leads to enhanced Coulomb interactions and an extraordinarily large exciton binding energy of a few hundred meV [10–17]. Individual single TMDs and other 2D material layers can be assembled into functional multilayer structures by van der Waals forces [5,8,18–20], with atomically sharp interfaces, digitally controlled layered components, and no lattice parameter constraints. Such van der Waals heterostructures exhibit remarkable properties such as spatially direct optical absorption but spatially indirect emission, and a strong interlayer coupling of charge carriers tunable by inserting dielectric layers [7,21]. The recent experimental observation of long-lived interlayer excitons in monolayer $MoSe_2$-WSe_2 heterostructures [8] opens an avenue to explore novel spin transport in these quasi-2D excitonic systems.

A paradigmatic example of spin transport is the spin Hall effect, which is receiving continuing and widespread interest in condensed matter physics, both theoretically [22–27] and experimentally [28–33]. Akin to the conventional Hall effect that gives charge current transverse to the applied electric field, the spin Hall effect generates transverse spin current and spin accumulation at the opposite edges of the samples. It can be understood as the deflection of the orbital motion by an effective gauge potential [24] arising from the spin-orbit coupling. In recent years, the spin Hall effect of electrons and holes in low-dimensional semiconductors has been intensively studied [25–27] and further generalized to photons [34–36] and cold atoms [37]. So far, most of the previous studies on the spin Hall effect of electrons and holes rely on the spin-orbit couplings and an electric field to drive the spin-dependent orbital motion. By contrast, the motion of charge-neutral excitons is difficult to control.

In this Letter, we propose a light-induced "spin" Hall effect for neutral, massive bosons, i.e., interlayer exciton gas in a monolayer $MoSe_2$-WSe_2 van der Waals heterostructure. Our scheme is based on two experimentally observed features of interlayer excitons: the long lifetime of about a few nanoseconds [8] (which allows for controlling the exciton transport before recombination), and the large binding energy [10–16] (which allows for strong exciton-laser interaction). The essential idea is to apply two spatially varying infrared laser beams coupled to the exciton internal levels in the V-type configuration to generate two laser-exciton dressed states (mapped to "spin-up" and "spin-down" states, respectively) that depend parametrically on the center-of-mass (c.m.) coordinate $\mathbf{R}$ of the exciton due to the $\mathbf{R}$-dependent laser-exciton interaction. Since the exciton spin dynamics is much faster than its c.m. motion, application of the Born-Oppenheimer approximation gives rise to a spin-dependent gauge field on the c.m. motion [27]. This gauge field, in turn, leads to spin-dependent deflection of the exciton c.m. motion and, hence, exciton spin Hall effect: a pure exciton spin current (but vanishing mass current) flowing transverse to the gauge field and laser propagation. In a Hall bar geometry, the nonuniform gauge field generates a series of spin-dependent chiral edge states. The exciton spin Hall

effect and the chiral edge states can be detected by spatially resolved photoluminescence spectroscopy.

The physical system under consideration is a monolayer $MoSe_2$-WSe_2 van der Waals heterostructure [8] [Fig. 1(a)]. The interlayer van der Waals interaction, which is much smaller than the band gaps of the monolayers, has a small influence on the band structure [38], as confirmed by our first-principles calculations (see Supplemental Material [39] for more details). This allows us to treat each monolayer as independent. For the ith layer ($i = 1$ for $MoSe_2$ and $i = 2$ for WSe_2), the low-energy single-particle Hamiltonian near the $\pm\mathbf{K}$ valleys is given by [2]

$$\hat{H}_i = a_i t_i(\tau k_x \sigma_x + k_y \sigma_y) + \frac{\Delta_i}{2}\sigma_z - \lambda_i \tau \frac{\sigma_z - 1}{2}\hat{s}_z, \quad (1)$$

with $\tau = \pm 1$ for $\mathbf{K}$ and $-\mathbf{K}$ valleys, $\sigma_z = \pm 1$ for the conduction and valence bands, and $\hat{s}_z = \pm 1$ for the physical spin of the electron. For $MoSe_2$, the bond length $a_1 = 3.313$ Å, nearest-neighbor hopping $t_1 = 0.94$ eV, band gap $\Delta_1 = 1.47$ eV, and valence-band spin-orbit coupling $\lambda_1 = 0.09$ eV. For WSe_2, we have $a_2 = 3.310$ Å, $t_2 = 1.19$ eV, $\Delta_2 = 1.60$ eV, and $\lambda_2 = 0.23$ eV. In Eq. (1), the spin-up and spin-down parts are completely decoupled. Under left (right) circularly polarized optical excitation, only the $\mathbf{K}$ ($-\mathbf{K}$) valley is populated [2,10], so we focus on one valley (say, the $\mathbf{K}$ valley) from now on. Because of the type-II band alignment [Fig. 1(b)], the optically generated electrons (holes) accumulate in the conduction (valence) band of $MoSe_2$ (WSe_2) and form interlayer excitions. For specificity, we consider A-type excitons consisting of a spin-up electron in the bottom layer and a spin-down hole in the top layer [2,10], as schematically shown in Fig. 1. To obtain internal energy level solutions, we transform the electron and hole positions $\mathbf{r}_e$ and $\mathbf{r}_h$ into the c.m. coordinate $\mathbf{R}$ and the internal coordinate $\mathbf{r} = \mathbf{r}_e - \mathbf{r}_h$ [39], so the exciton Hamiltonian is the sum of the c.m. part $\hat{\mathbf{P}}^2/(2M)$, band edge energy $(\Delta_1 + \Delta_2 - 2\lambda_2)/2$, and the internal part

$$\hat{H}_{\text{in}} = -\frac{\hbar^2}{2m_r}\nabla_{\mathbf{r}}^2 + V(\mathbf{r}),$$

where $M(\epsilon) = m_1(\epsilon) + m_2(\epsilon)$ and $m_r(\epsilon) = m_1(\epsilon)m_2(\epsilon)/M(\epsilon)$ are the exciton total mass and reduced mass, respectively [39]. m_1 and m_2 are the masses of the electron and hole, respectively, as defined in the Supplemental Material [39]. $V(\mathbf{r}) = -e^2/(4\pi\varepsilon\varepsilon_0\sqrt{r^2 + d^2})$ is the electron-hole Coulomb attraction, with dielectric constant $\epsilon = 2.3$ [21] and interlayer distance $d = 0.73$ nm. Numerically diagonalizing $\hat{H}_{\text{in}}$ gives the exciton ground state $|1s\rangle$ (energy -345 meV) and a few excited states of the internal dynamics, such as the nondegenerate $|2s\rangle$ and doubly degenerate $\{|2p_x\rangle, |2p_y\rangle\}$ (energy -56 meV) and $\{|3p_x\rangle, |3p_y\rangle\}$ (energy -29 meV), similar to 2D hydrogen atom eigenstates.

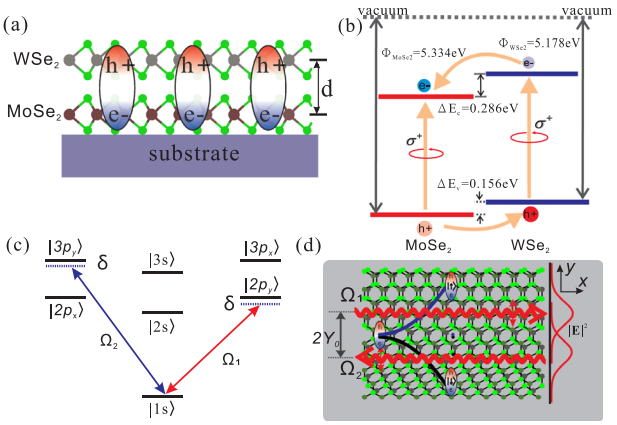

FIG. 1 (color online). Schematic of interlayer exciton gas in a monolayer $MoSe_2$-WSe_2 van der Waals heterostructure with distance $d = 0.73$ nm between Mo and W atom layers. (a) Spatially separated interlayer exciton due to type-II band alignment shown in (b). (b) Band alignment and work functions of $MoSe_2$-WSe_2 van der Waals heterostructure from first-principles calculations. The work functions of $MoSe_2$ and WSe_2 are 5.334 and 5.178 eV, respectively. The band offsets indicate a type-II band alignment. (c) Two infrared laser beams linearly polarized along the y axis couple three internal states of the interlayer exciton into a V-type configuration, with different Rabi frequencies Ω_1 and Ω_2 with the same detuning δ. (d) Configuration of the two Gaussian laser beams, counterpropagating nearly parallel to the surface (i.e., large incident angle) with shifted centers.

We choose the exciton ground state $|g\rangle \equiv |1s\rangle$ and two low excited states $|1\rangle \equiv |2p_y\rangle$ and $|2\rangle \equiv |3p_y\rangle$ to form a V-type three-level configuration, as shown in Fig. 1(b). Two infrared laser beams propagating along the x axis and linearly polarized along the y axis are applied to couple $|g\rangle$ to $|1\rangle$ and $|2\rangle$, respectively, with equal detuning δ [see Fig. 1(c)] and spatially varying Rabi frequencies $\Omega_\lambda(\mathbf{R})$ and phases $\phi_\lambda(\mathbf{R})$ $(\lambda = 1, 2)$ defined via $\hbar\Omega_\lambda e^{i\phi_\lambda} = eE_\lambda(\mathbf{R})\langle g|\mathbf{e}_y \cdot \mathbf{r}|\lambda\rangle$, where $|\langle g|\mathbf{e}_y \cdot \mathbf{r}|1\rangle| \simeq 0.136$ nm and $|\langle g|\mathbf{e}_y \cdot \mathbf{r}|2\rangle| \simeq 0.065$ nm. Such a three-level system has been widely studied for electromagnetically induced transparency [48] and optical coupling between the two excited states [49]. Here we utilize the formation of a dark state and a bright state in the V-type configuration to generate spin-dependent gauge field to drive the spin Hall effect for interlayer excitons. In the presence of laser excitation, the exciton internal Hamiltonian H_{in} is

$$H_{\text{in}} = \frac{\hbar}{2}\begin{pmatrix} 0 & \Omega_1(\mathbf{R})e^{i\phi_1(\mathbf{R})} & \Omega_2(\mathbf{R})e^{i\phi_2(\mathbf{R})} \\ \Omega_1(\mathbf{R})e^{-i\phi_1(\mathbf{R})} & 2\delta & 0 \\ \Omega_2(\mathbf{R})e^{-i\phi_2(\mathbf{R})} & 0 & 2\delta \end{pmatrix}. \quad (2)$$

For large positive detuning $\delta \gg \Omega \equiv (\Omega_1^2 + \Omega_2^2)^{1/2}$, two eigenvalues $\lambda_\downarrow = \hbar\delta$ and $\lambda_\uparrow(\mathbf{R}) \approx \hbar\delta + \hbar\Omega^2/(4\delta)$ are energetically far from the third eigenvalue

$\lambda_g(\mathbf{R}) \approx -\hbar\Omega^2/(4\delta)$; the corresponding eigenstates (dressed states) $|\chi_\downarrow(\mathbf{R})\rangle \propto \cos\theta|1\rangle - \sin\theta e^{i\phi(\mathbf{R})}|2\rangle$ and $|\chi_\uparrow(\mathbf{R})\rangle \propto \sin\theta e^{-i\phi(\mathbf{R})}|1\rangle + \cos\theta|2\rangle$ form a two-level system, with $|\chi_\downarrow(\mathbf{R})\rangle$ and $|\chi_\uparrow(\mathbf{R})\rangle$ identified as the spin-down and spin-up states, respectively. Here $\phi(\mathbf{R}) \equiv \phi_1(\mathbf{R}) - \phi_2(\mathbf{R})$ and $\theta = \tan^{-1}(\Omega_1/\Omega_2)$. When the coupling between opposite spin states is small, i.e., when the two-photon Doppler detuning $\Pi = \cos^2\theta|\mathbf{v}\cdot\nabla(\tan\theta e^{i\phi(\mathbf{R})})|$ ($\mathbf{v}$ is the typical exciton velocity) is much smaller than the spin gap $|\lambda_\uparrow - \lambda_\downarrow| \simeq \hbar\Omega^2/4\delta$, we can neglect the spin-flip transitions (i.e., the Born-Oppenheimer approximation) and we obtain an effective c.m. Hamiltonian [39]

$$H_\sigma = \frac{1}{2M}(\mathbf{P} - \mathbf{A}_\sigma)^2 + V_\sigma \tag{3}$$

associated with different spin states $\sigma = \uparrow$ and $\downarrow$, where

$$\mathbf{A}_\sigma = i\hbar\langle\chi_\sigma|\nabla_\mathbf{R}|\chi_\sigma\rangle = \pm\hbar\sin^2\theta\nabla_\mathbf{R}\phi(\mathbf{R})$$

("+" for $\mathbf{A}_\uparrow$ and "−" for $\mathbf{A}_\downarrow$) is the vector potential and $V_\sigma(\mathbf{R}) = \lambda_\sigma + W(\mathbf{R})$, with $W(\mathbf{R}) = (\hbar^2/2M)[|\nabla_\mathbf{R}\theta|^2 + \sin^2\theta\cos^2\theta|\nabla_\mathbf{R}\phi(\mathbf{R})|^2]$. This spin-dependent gauge potential originates from the parametric dependence of the spin states on the c.m. coordinate $\mathbf{R}$ of the exciton, leading to spin-dependent deflection of the c.m. motion; e.g., the effective gauge field

$$\mathbf{B}_\sigma = \nabla_\mathbf{R}\times\mathbf{A}_\sigma = \eta_\sigma\hbar\sin(2\theta)\nabla_\mathbf{R}\theta\times\nabla_\mathbf{R}\phi(\mathbf{R}) \tag{4}$$

on the c.m. motion is opposite for opposite exciton spin, a critical ingredient for achieving the exciton spin Hall effect. For specificity, now we consider two counterpropagating Gaussian laser beams with shifted centers along the y axis and spatial profiles $eE_\lambda(\mathbf{R})\langle g|\mathbf{e}_y\cdot\mathbf{r}|\lambda\rangle/\hbar = \Omega_\lambda(\mathbf{R})e^{i\phi_\lambda(\mathbf{R})} = \Omega_0\exp[-(Y-Y_\lambda)^2/a^2]\exp(ik_\lambda X)$ ($\lambda = 1, 2$), where $\mathbf{R} = (X, Y)$ and the center positions $Y_1 = -Y_2 = Y_0$, as shown in Fig. 1(d). This generates a spatially varying gauge field

$$\mathbf{A}_\sigma = \frac{\eta_\sigma\hbar(|k_1| + |k_2|)}{1 + e^{-Y/l}}\mathbf{e}_x, \qquad \mathbf{B}_\sigma = \frac{-\eta_\sigma\hbar(|k_1| + |k_2|)}{4l\cosh^2(Y/2l)}\mathbf{e}_z$$

($l = a^2/8Y_0$) that gives rise to a spin Hall current for excitons, as we demonstrate below. In subsequent calculations, we use the following realistic parameters: laser beam width $a = 10\ \mu$m, spatial shift $Y_0 = 2.5\ \mu$m, detuning $\hbar\delta = 1$ meV, and Rabi frequency $\hbar\Omega_0 = 150\ \mu$eV. For a Gaussian laser beam with intensity distribution in the waist plane $\epsilon_0 c|E(r)|^2/2 = I_0\exp(-2r^2/a^2)$, the average power is $P = \pi I_0 a^2/2$. Thus, the Rabi frequency $\hbar\Omega_0 = 150\ \mu$eV for the λth laser beam ($\lambda = 1, 2$) corresponds to the average power $P_\lambda = \pi\hbar^2 a^2\Omega_0^2\epsilon_0 c/(4\eta e^2|\langle g|\mathbf{e}_y\cdot\mathbf{r}|\lambda\rangle|^2)$, i.e., $P_1 = 0.254$ W for laser beam 1 and $P_2 = 1.113$ W for laser beam 2, which are both experimentally achievable. The above parameters correspond to $|k_1| + |k_2| \approx 3\ \mu\text{m}^{-1}$, exciton total mass $M \approx 0.64m_e$ (m_e is the free electron mass), and exciton spin splitting $|\lambda_\uparrow - \lambda_\downarrow| = 10\ \mu$eV at $Y = 0$. For typical velocity of exciton $|\mathbf{v}| \ll 10$ km/s or the corresponding wave vector $k \ll M|\mathbf{v}|/\hbar = 50\ \mu\text{m}^{-1}$, the two-photon Doppler detuning $\Pi \ll |\lambda_\uparrow - \lambda_\downarrow|$, so that the spin-flip transitions are suppressed and the Born-Oppenheimer approximation is justified. The typical gauge field $B_\sigma \sim 1$ Gs.

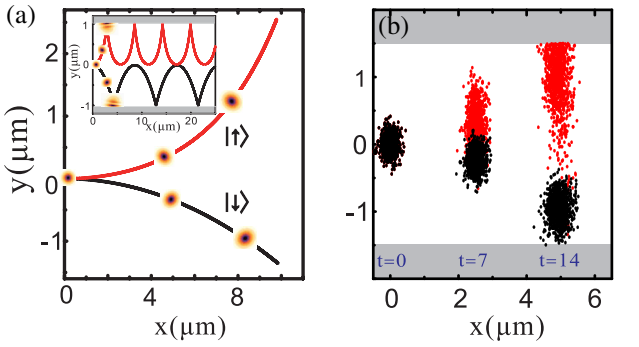

FIG. 2 (color online). Laser-induced spin-dependent deflection of (a) a single exciton with initial velocity $v_{x0} = 1\ \mu$m/ns and (b) an exciton gas with initial mean velocity $v_{x0} = 0.35\ \mu$m/ns along the x axis in a Hall bar structure with $L = 3\ \mu$m along the y axis. The colored clouds depict the evolution of spin-up and spin-down Gaussian wave packets, which coincides with the classical trajectories. The inset of panel (a) gives the spin-dependent skipping motion of the exciton with an initial velocity $v_{x0} = 0.3\ \mu$m/ns in a Hall bar with $L = 2\ \mu$m along the y axis. In (b), the red and black dots depict the spin-up and spin-down excitons. The width of the initial spatial (velocity) distribution of the exciton gas is $\xi_R = 0.25\ \mu$m ($\xi_v = 0.01\ \mu$m/ns) and the evolution of the spatial density profiles are shown at $t = 0$, 7, and 14 ns.

Now we propose an experimental setup to detect the spin Hall current in excitonic gas subjected to the above configuration of laser-exciton coupling. Suppose that at $t = 0$ an exciton moves along the x axis (this can be achieved by a temperature difference or by injecting excitons into the sample) and the exciton internal state is a superposition of spin-up and spin-down dressed states $|\chi_\uparrow\rangle$ and $|\chi_\downarrow\rangle$. In the presence of the spin-dependent gauge field, the exciton canonical momentum along the x axis remains constant,

$$\dot{X}_\sigma = (P_\sigma^x - A_\sigma)/M, \qquad \dot{P}_\sigma^x = 0, \tag{5}$$

but the exciton acquires a spin-dependent transverse velocity along the y axis,

$$\dot{Y}_\sigma = P_\sigma^y/M, \qquad \dot{P}_\sigma^y = \frac{P_\sigma^x - A_\sigma}{M}\partial_Y A_\sigma - \partial_Y V_\sigma. \tag{6}$$

As shown in Fig. 2(a), the typical exciton trajectories under the gauge field depends on the exciton spin state σ, leading

to a spin Hall current in the y axis in the case of many excitons. We also investigate the evolution of a Gaussian wave packet governed by the Hamiltonian in Eq. (3). The quantum motion conforms to the classical trajectories, as shown in Fig. 2(a). Note that the asymmetry of the spin-dependent trajectories (black and red lines) arises from the spin-dependent potential V_σ.

To model the spin Hall current produced by the motion of a laser-generated dilute exciton gas, we assume that at $t = 0$, the c.m. coordinate and velocity of the exciton gas obey the Gaussian distribution $\rho_R(\mathbf{R}) = (2\pi\xi_R^2)^{-1}\exp[-(X^2+Y^2)/2\xi_R^2]$ and $\rho_v(v_x, v_y) = (2\pi\xi_v^2)^{-1}\exp\{-[(v_x - v_{x0})^2 + v_y^2]/2\xi_v^2\}$, respectively. The variances ξ_R and ξ_v account for the quantum uncertainties and classical broadening due to the finite temperature and the intensity distribution of the light that generates the exciton gas. The evolution of the density profile of the exciton gas is simulated numerically by solving Eqs. (5) and (6), and the results are shown in Fig. 2(b). The results clearly demonstrate a spin-dependent flow of the exciton gas and, hence, spin Hall current along the y axis due to the spin-dependent gauge field. In our system, the lifetime of excitons is about a few nanoseconds [8], which is comparable to the exciton separation time, as shown in Fig. 2(b). In a Hall bar geometry with a finite width along the y direction, the excitons with opposite spins would accumulate along the opposite boundaries and then recombine, as shown in Fig. 2(b). This allows the exciton spin Hall effect to be detected by spatially resolved photoluminescence spectroscopy [8,50,51].

Now we prove that the spin-dependent gauge field gives rise to chiral edge states in a Hall bar structure, with a finite width $L = 4$ μm along the y direction. The exciton c.m. wave function $\Psi_\sigma(X, Y) = e^{ik_x X}\varphi_\sigma(Y)$, where $\varphi_\sigma(Y)$ is governed by the effective Hamiltonian

$$H_{k_x}^\sigma = \frac{\hbar^2}{2M}\left\{[k_x - A_\sigma(Y)]^2 - \frac{d^2}{dY^2}\right\} + V_\sigma(Y), \qquad (7)$$

which can be numerically diagonalized. The resulting spin-dependent dispersion relation and density distribution of edge states is shown in Fig. 3. For spin-up (spin-down) states, the minimum energy of the c.m. motion occurs at k_0 ($-k_0$) with $k_0 = (|k_1| + |k_2|)/2 \approx 1.5$ μm^{-1}. In the Hall bar region, the gauge field has a characteristic magnetic length $l_B = \sqrt{\hbar/|B_\sigma|} \simeq 2$ μm, comparable to the Hall bar width L. Consequently, during the gauge field induced cyclotron motion, the exciton frequently collides at the Hall bar boundary. This feature prevents the formation of well-defined Landau levels, but instead gives rise to chiral edge states, similar to the quantum Hall effect. However, the spin dependence of the gauge field gives an additional feature: the spin-velocity locking. As shown in Fig. 3, in the upper edge of the Hall bar, the lowest spin-down edge state [blue curve in Fig. 3(a)] propagates from the right to the left,

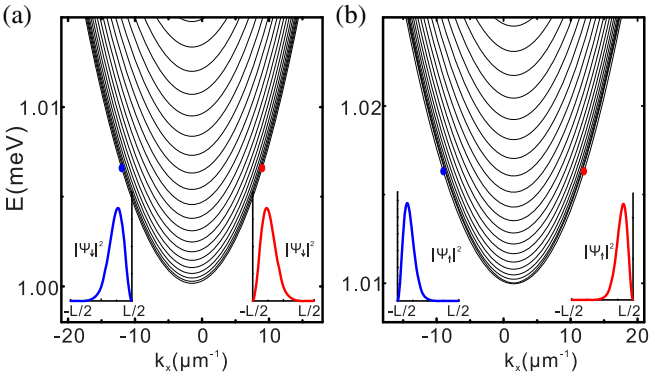

FIG. 3 (color online). Dispersion relation of the exciton c.m. motion in a 4-μm Hall bar for (a) spin-down and (b) spin-up excitons. The inset at the bottom of each panel gives the spatial profile of the lowest chiral edge states (as marked by filled circles in the dispersion curve).

while the lowest spin-up edge state [red curve in Fig. 3(b)] propagates in the opposite direction. This gives a vanishing mass current $j_m = j_\uparrow + j_\downarrow$ but finite spin current $j_s = j_\uparrow - j_\downarrow = 2j_\uparrow$, flowing from the left to the right along the upper edge of the Hall bar. Similarly, in the lower edge of the Hall bar, the right-going spin-down edge states [red curve in Fig. 3(a)] and the left-going spin-up edge states [blue curve in Fig. 3(b)] give a vanishing mass current but finite spin current flow from the right to the left (opposite to the spin current flow in the upper edge).

Finally, we briefly discuss the experimental generation and detection of the chiral edge states and spin current. To neglect the Coulomb interaction between excitons, we use a dilute exciton gas and detect above the temperature of Bose-Einstein condensation. To generate the chiral edge states or spin current, we can generate an effective electrical field along the x axis, e.g., by keeping the two terminals of the sample at different temperatures, so that the temperature gradient $\nabla(1/T)\|\mathbf{e}_x$ would drive the optically generated excitons to diffuse along the x axis. Then we can detect the spin current by spatially resolved photoluminescence spectroscopy [8,50,51]. To increase the lifetime of interlayer excitons for more pronounced effect, we could apply a perpendicular electrical field or place a 2D dielectric material between the $MoSe_2$ and WSe_2 layers.

In summary, we have proposed an optically induced spin Hall effect for interlayer exciton gas of a monolayer $MoSe_2$-WSe_2 van der Waals heterostructure. The essential physics is to apply two spatially varying laser beams coupled to the exciton internal levels to generate a spin-dependent gauge field on the exciton center-of-mass motion, which deflects excitons in different spin states in opposite directions. This gives rise to a finite exciton spin Hall current in an ensemble of noninteracting exciton gas, and chiral edge states with spin-velocity locking in a Hall bar structure. This light-induced gauge potential on long-lived excitons makes excitonic systems a new platform for

exploring various Hall physics and their interplay with exciton-exciton interactions and temperatures.

This work was supported by Grants No. 2011CB922204-2 and No. 2015CB921503 from the MOST of China, and NSFC Grants No. 11434010, No. 11274036, and No. 11322542.

*Corresponding author.
kchang@semi.ac.cn

[1] K. F. Mak, C. Lee, J. Hone, J. Shan, and T. F. Heinz, Phys. Rev. Lett. **105**, 136805 (2010).
[2] D. Xiao, G. B. Liu, W. Feng, X. Xu, and W. Yao, Phys. Rev. Lett. **108**, 196802 (2012).
[3] Q. H. Wang, K. Kalantar-Zadeh, A. Kis, J. N. Coleman, and M. S. Strano, Nat. Nanotechnol. **7**, 699 (2012).
[4] H. Zeng, J. Dai, W. Yao, D. Xiao, and X. Cui, Nat. Nanotechnol. **7**, 490 (2012).
[5] A. K. Geim and I. V. Grigorieva, Nature (London) **499**, 419 (2013).
[6] L. Britnell, A. H. Castro Neto, K. S. Novoselov *et al.*, Science **340**, 1311 (2013).
[7] H. Fanga, C. Battaglia, A. Javey *et al.*, Proc. Natl. Acad. Sci. U.S.A. **111**, 6198 (2014).
[8] P. Rivera, W. Yao, X. D. Xu *et al.*, Nat. Commun. **6**, 6242 (2015).
[9] F. Withers, A. Mishchenko, K. S. Novoselov *et al.*, Nat. Mater. **14**, 301 (2015).
[10] K. F. Mak, K. He, C. Lee, G. H. Lee, J. Hone, T. F. Heinz, and J. Shan, Nat. Mater. **12**, 207 (2013).
[11] M. M. Ugeda, A. J. Bradley, S.-F. Shi, and M. F. Crommie, Nat. Mater. **13**, 1091 (2014).
[12] J. S. Ross, W. Yao, X. D. Xu *et al.*, Nat. Commun. **4**, 1474 (2013).
[13] K. He, N. Kumar, L. Zhao, Z. Wang, K. F. Mak, H. Zhao, and Jie Shan, Phys. Rev. Lett. **113**, 026803 (2014).
[14] A. Chernikov, T. C. Berkelbach, H. M. Hill, A. Rigosi, Y. Li, O. B. Aslan, D. R. Reichman, M. S. Hybertsen, and T. F. Heinz, Phys. Rev. Lett. **113**, 076802 (2014).
[15] Z. Ye, T. Cao, K. O'Brien, H. Zhu, X. Yin, Y. Wang, S. G. Louie, and X. Zhang, Nature (London) **513**, 214 (2014).
[16] B. Zhu, X. Chen, and X. D. Cui, Sci. Rep. **5**, 9218 (2015).
[17] T. Stroucken and S. W. Koch, arXiv:1404.4238.
[18] L. A. Ponomarenko, A. K. Geim, R. V. Gorbachev *et al.*, Nat. Phys. **7**, 958 (2011).
[19] S. J. Haigh, A. Gholinia, R. Jalil, S. Romani, L. Britnell, D. C. Elias, K. S. Novoselov, L. A. Ponomarenko, A. K. Geim, and R. Gorbachev, Nat. Mater. **11**, 764 (2012).
[20] T. Georgiou, R. Jalil, A. Mishchenko *et al.*, Nat. Nanotechnol. **8**, 100 (2013).
[21] M. M. Fogler, L. V. Butov, and K. S. Novoselov, Nat. Commun. **5**, 4555 (2014); A. Kumar and P. K. Ahluwalia, Physica (Amsterdam) **407B**, 4627 (2012).
[22] M. I. Dyakonov and V. I. Perel, JETP Lett. **13**, 467 (1971).
[23] J. E. Hirsch, Phys. Rev. Lett. **83**, 1834 (1999); S. Zhang, Phys. Rev. Lett. **85**, 393 (2000).
[24] S. Murakami, N. Nagaosa, and S. Zhang, Science **301**, 1348 (2003); S. Murakami, N. Nagaosa, and S. C. Zhang, Phys. Rev. Lett. **93**, 156804 (2004).
[25] J. Sinova, D. Culcer, Q. Niu, N. A. Sinitsyn, T. Jungwirth, and A. H. MacDonald, Phys. Rev. Lett. **92**, 126603 (2004).
[26] W. Yang, K. Chang, and S. C. Zhang, Phys. Rev. Lett. **100**, 056602 (2008).
[27] L. K. Shi, S. C. Zhang, and K. Chang, Phys. Rev. B **87**, 161115(R) (2013).
[28] Y. K. Kato, R. C. Myers, A. C. Gossard, and D. D. Awschalom, Science **306**, 1910 (2004).
[29] J. Wunderlich, B. Kaestner, J. Sinova, and T. Jungwirth, Phys. Rev. Lett. **94**, 047204 (2005).
[30] T. Kimura, Y. Otani, T. Sato, S. Takahashi, and S. Maekawa, Phys. Rev. Lett. **98**, 156601 (2007).
[31] N. P. Stern, S. Ghosh, G. Xiang, M. Zhu, N. Samarth, and D. D. Awschalom, Phys. Rev. Lett. **97**, 126603 (2006).
[32] H. Zhao, E. J. Loren, H. M. van Driel, and A. L. Smirl, Phys. Rev. Lett. **96**, 246601 (2006).
[33] N. P. Stern, D. Steuerman, and D. D. Awschalom, Nat. Phys. **4**, 843 (2008).
[34] O. Hosten and P. Kwiat, Science **319**, 787 (2008).
[35] J. Korger, A. Aiello, V. Chille, P. Banzer, C. Wittmann, N. Lindlein, C. Marquardt, and G. Leuchs, Phys. Rev. Lett. **112**, 113902 (2014).
[36] K. Fang, Z. Yu, and S. Fan, Nat. Photonics **6**, 782 (2012).
[37] S. L. Zhu, H. Fu, C. J. Wu, S. C. Zhang, and L. M. Duan, Phys. Rev. Lett. **97**, 240401 (2006).
[38] H. Yu, Y. Wang, Q. J. Tong, X. D. Xu, and W. Yao, arXiv:1504.01215.
[39] See Supplemental Material at http://link.aps.org/supplemental/10.1103/PhysRevLett.115.166804 for details of our calculation and derivation, which includes Refs. [40–47].
[40] P. Hohenberg and W. Kohn, Phys. Rev. B **136**, B864 (1964).
[41] G. Kresse and J. Furthmuller, Phys. Rev. B **54**, 11169 (1996).
[42] G. Kresse and D. Joubert, Phys. Rev. B **59**, 1758 (1999).
[43] J. P. Perdew, K. Burke, and M. Ernzerhof, Phys. Rev. Lett. **77**, 3865 (1996).
[44] J. P. Perdew and Y. Wang, Phys. Rev. B **33**, 8800 (1986).
[45] H. J. Monkhorst and J. D. Pack, Phys. Rev. B **13**, 5188 (1976).
[46] S. Grimme, J. Comput. Chem. **27**, 1787 (2006).
[47] P. O. Löwdin, J. Chem. Phys. **19**, 1396 (1951).
[48] J. P. Marangos, J. Mod. Opt. **45**, 471 (1998).
[49] X. J. Liu, K. T. Law, and T. K. Ng, Phys. Rev. Lett. **112**, 086401 (2014).
[50] V. K. Sangwan, D. Jariwala, I. S. Kim, K. S. Chen, T. J. Marks, L. J. Lauhon, and M. C. Hersam, Nat. Nanotechnol. **10**, 403 (2015).
[51] S. Bieker, T. Henn, T. Kiessling, W. Ossau, and L. W. Molenkamp, Phys. Rev. Lett. **114**, 227402 (2015).